TECHNICAL REPORT R-86

THE DRAG COEFFICIENT OF PARABOLIC BODIES OF REVOLUTION OPERATING AT ZERO CAVITATION NUMBER AND ZERO ANGLE OF YAW

By VIRGIL E. JOHNSON, JR., and THOMAS A. RASNICK

Langley Research Center
Langley Field, Va.

TECHNICAL REPORT R-86

THE DRAG COEFFICIENT OF PARABOLIC BODIES OF REVOLUTION OPERATING AT ZERO CAVITATION NUMBER AND ZERO ANGLE OF YAW

By Virgil E. Johnson, Jr., and Thomas A. Rasnick

SUMMARY

The drag coefficient of parabolic bodies of revolution with fineness ratios greater than 1 operating at zero angle of yaw and zero cavitation number is determined both theoretically and experimentally. The theoretical analysis is an approximate one which utilizes the theoretical pressure distribution on the positive pressure region of thin elliptical bodies of revolution. Results of an experimental investigation on two paraboloids having fineness ratios of 1.00 and 3.33 are also presented. Zero cavitation number was approximated in the experiments by ventilating the base of the bodies to the atmosphere while operating at speeds up to 190 fps. The experimental drag coefficients are shown to be in excellent agreement with the theory. The theoretical form-drag coefficient of paraboloids operating at zero cavitation number is found to be about one-half the form-drag coefficient of cones having the same fineness ratio.

INTRODUCTION

When a body is moved through a liquid at very high speeds, low-pressure regions of the liquid may reach the vapor pressure and boil or cavitate. The influence of this cavitation on the body is to increase the form drag above that for the noncavitating body and to cause damage to the walls of the body if the condition is such that the cavities collapse on the wall. At a given depth of submersion the only way of preventing cavitation from occurring is to make the body fine enough so that the minimum pressure in the flow field does not reach the vapor pressure at the design speed. However, if the design speed is very high (200 to 300 knots) and the ambient pressure is low (shallow depth of submersion) the body fineness ratio may become impractically large. Thus, if cavitation cannot be feasibly avoided at high speeds the shape of the body should at least be designed to operate without surface damage and with as low a drag as possible.

A high-speed body free from cavitation damage at zero angle of yaw may be accomplished by confining the negative pressure regions to the wake of a blunt base and contouring the surface forward of the base so as to produce only positive pressure coefficients. The result at high speeds will be a fully wetted body forward surface followed by a very long vapor-filled cavity emanating from the end of the body. If the speed is sufficiently high, the end of this cavity will be far removed from the base of the body and no damage to the body surface will occur.

Body shapes which would produce this supercavitating type of operation at zero angle of yaw are cones and paraboloids with blunt bases. The form-drag coefficient of cones operating with base cavities has been known for several years. However, the drag coefficient of paraboloids operating with base cavities has not been heretofore determined except for the trivial case of infinite fineness ratio. Since parabolic struts are known to have less drag than wedge-shaped struts, paraboloids are expected to have less drag than cones.

The purpose of the present investigation is to determine both theoretically and experimentally the magnitude of the form-drag coefficient of paraboloids of finite fineness ratios operating at zero angle of yaw with a base cavity whose pressure coefficient or cavitation number is zero.

SYMBOLS

a	semi-major axis of ellipse
b	semi-minor axis of ellipse
C_D	form-drag coefficient at arbitrary cavitation number, $\frac{D}{\frac{1}{2}\rho V^2 A}$
$C_{D,o}$	form-drag coefficient at zero cavitation number, $\frac{D_o}{\frac{1}{2}\rho V^2 A}$
C_p	pressure coefficient, $\frac{p-p_\infty}{\frac{1}{2}\rho V^2}$
$C_{p,min}$	minimum pressure coefficient, $\frac{p_{min}-p_\infty}{\frac{1}{2}\rho V^2}$
D	form drag at arbitrary cavitation number, lb
D_o	form drag at zero cavitation number, lb
d	base diameter of model
f	fineness ratio, $l/d=x_o/2y_o$
l	length of model
p	local pressure, lb/sq ft
p_∞	pressure in the undisturbed flow, lb/sq ft
p_c	cavity pressure, lb/sq ft
p_{min}	minimum pressure, lb/sq ft
R	axis ratio of ellipse, a/b
A	base area, sq ft
V	speeds, fps
x,y	Cartesian coordinates, origin at body nose
x_o,y_o	Cartesian coordinates of location of zero pressure coefficient
$y'=y/y_o$	
ρ	mass density of water, lb-sec^2/ft^4
σ	cavitation number, $\frac{p_\infty-p_c}{\frac{1}{2}\rho V^2}$

THEORY

BACKGROUND

At sufficiently high speeds the amount of cavitation occurring on a body may be so great that the rearward portion of the body becomes completely unwetted and enclosed in a long trailing cavity as shown in figure 1(a). It is well known that the most significant dimensionless parameter which defines this supercavitating flow is the cavitation number. The cavitation number, denoted as σ, is the negative of the pressure coefficient in the unwetted region; that is,

$$\sigma=\frac{p_\infty-p_c}{\frac{1}{2}\rho V^2}$$

where p_∞ is the pressure in the undisturbed flow, p_c is the pressure within the cavity, ρ is the fluid density, and V is the speed of the body.

The length of the cavity formed behind the wetted portion of the body increases as the cavitation number is decreased and approaches infinite length at zero cavitation number. The unwetted portion of a supercavitating body has no effect on the flow and may be removed, leaving a blunt-based nosepiece or forebody followed by a long cavity, as shown in figure 1(b). The equation defining the cavitation number shows that very low values of the cavitation number may result either when the speed is extremely high or when the cavity pressure p_c approaches the ambient pressure p_∞, or when both conditions occur. For example, a blunt-based rocket-powered torpedo may operate at very shallow depths in a condition approaching zero cavitation number because of its high speed and because the cavity pressure is increased by rocket gases.

In reference 1 it is pointed out that the two-dimensional thin strut section which has near minimum drag at zero cavitation number for a given ratio of base thickness to chord is parabolic in shape. This conclusion is based on the knowledge that the asymptotic shape of the cavity formed behind any two-dimensional obstacle at zero cavitation number is parabolic. Consequently, a thin strut constructed to fit the asymptotic shape would be expected to have low drag because over a large percentage of its chord the pressure coefficient would be zero and contribute no drag. The drag coefficient of a two-dimensional parabolic strut is determined by linearized methods in reference 1.

It is shown in reference 2 that the asymptotic shape of the cavity formed behind an axisymmetric body operating at zero cavitation number is given by the equation

$$y=\frac{Cx^{1/2}}{(\log_e x)^{1/4}} \qquad (1)$$

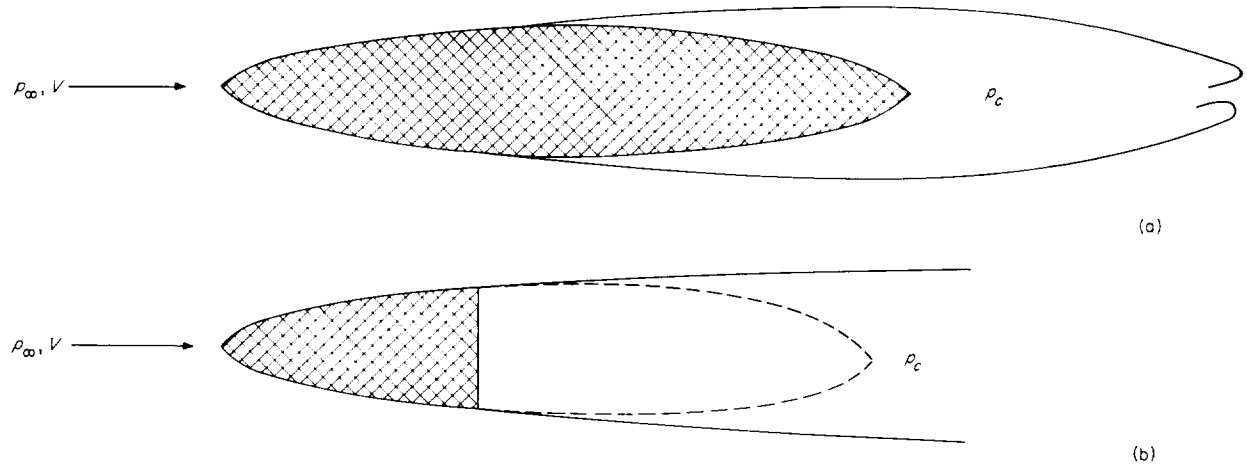

(a) Finite cavitation number (V, finite; $p_\infty > p_c$).
(b) Zero cavitation number ($V=\infty$ or $p_\infty = p_c$).

FIGURE 1.—Definition sketch.

where C is a constant. This equation cannot be used to describe completely a low-drag body shape because of the peculiar behavior of the function near $x=1$. However, for any practical fineness ratio a parabola may be found which is an excellent approximation to equation (1) for $x>2$, and the parabola provides a practical nose region. Consequently, of all possible thin axisymmetric shapes operating at zero cavitation number, a parabolic body of revolution would be expected to possess a near-minimum drag. The magnitude of the drag coefficient of such bodies is needed for design purposes.

The solution for the pressure distribution on a parabolic half-body (body with infinite length) may be found in practically all hydrodynamic textbooks; however, except for the trivial case of the paraboloid of infinite fineness ratio operating at zero cavitation number, the half-body solution is not useful.

An analysis leading to an approximate solution for the drag coefficient of paraboloids of finite fineness ratios operating at zero angle of yaw and zero cavitation number is presented in the following section along with a similar analysis for the two-dimensional case.

ANALYSIS

Parabolic bodies of revolution.—The method presented for determining theoretically the drag coefficient of parabolic bodies of revolution with finite fineness ratios operating at zero cavitation number is an approximate one. The method utilizes the result obtained in reference 3 that the cavity shape behind an axisymmetric body at finite cavitation number is very nearly elliptical and the result obtained for conical bodies in reference 4 that for relatively thin cones the drag coefficient for small cavitation numbers is approximately $C_{D,o}+\sigma$, where $C_{D,o}$ is the drag coefficient at zero cavitation number. The result from reference 4 may be interpreted to mean that the pressure distribution on relatively thin bodies of revolution (exclusive of the base) is not significantly affected by changes in cavitation number. Therefore, the drag coefficient for thin bodies is increased by an increase in cavitation number only because of the change in pressure coefficient over the base. This statement is not true for thick bodies, because for thick bodies the drag coefficient at small cavitation numbers is known to be $C_{D,o}(1+\sigma)$. (See ref. 4.)

The theoretical pressure distributions on elliptical bodies of revolution having axis ratios of 10 and 20 are shown in figures 2(a) and 2(b), respectively. The distributions shown in figure 2 are computed from the theory given in references 5 and 6. The region of the ellipsoids forward of the point where the pressure coefficient is zero is shaded in these figures. It may be noted that downstream of the zero point the pressure coefficient is negative by a small and almost uniform amount. Thus, the pressure distribution shown is a fair approximation to the pressure distribution which would occur if the shaded nosepiece were

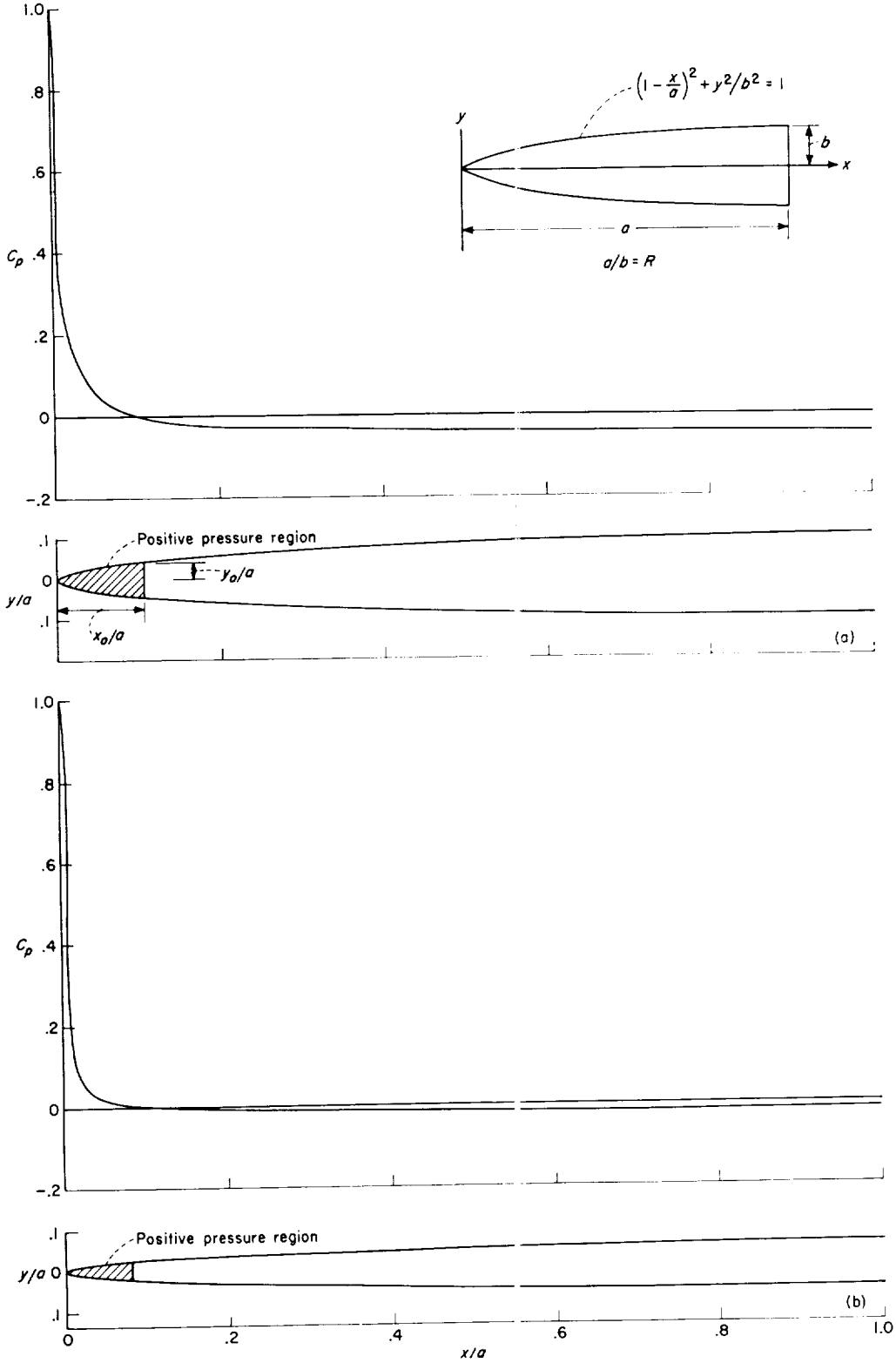

(a) $R=10$.
(b) $R=20$.

FIGURE 2.—Theoretical pressure distribution on ellipses.

operating at a small but finite cavitation number about equal to $-C_{p,min}$. Therefore, the pressure distribution forward of the zero point is essentially the same as that which would occur at zero cavitation number.

If the pressure distribution forward of the zero point is integrated over the shaded region to obtain the drag, this drag is approximately equal to the drag of the nosepiece operating at zero cavitation number. Furthermore, if the length of the nosepiece is relatively small compared with the semi-major axis of the ellipse, the nosepiece may be considered to be a close approximation to a paraboloid. It may be shown that as the fineness ratio of the parent ellipse approaches infinity the nosepiece becomes exactly a paraboloid which is also of infinite fineness ratio. Therefore, the approximate solution obtained by the method described becomes increasingly accurate for finer paraboloids and in the limit approaches the exact solution.

The flow field about an elliptical body of revolution in a uniform stream may be found in practically any textbook on hydrodynamics; for example, see reference 5 for the solution in elliptic coordinates. In Cartesian coordinates (with the origin at the body nose) the pressure coefficient for an elliptical body of revolution at zero angle of yaw may be determined as (see ref. 6)

$$C_p=1-K^2\frac{R^2\left(\frac{y}{b}\right)^2}{1+\left(\frac{y}{b}\right)^2(R^2+1)} \tag{2}$$

where

$$K=\frac{2\left(\frac{R^2-1}{R^2}\right)^{3/2}}{2\left(\frac{R^2-1}{R^2}\right)^{1/2}+\frac{1}{R^2}\log_e\frac{R+\sqrt{R^2-1}}{R-\sqrt{R^2-1}}}$$

R axis ratio of the ellipse a/b
a semi-major axis of the ellipse
b semi-minor axis of the ellipse

The value of K varies from 1.5 to 1.0 as R varies from 1 to ∞.

Let the value of y at the point where $C_p=0$ be denoted as y_o. Then, if C_p is set equal to zero and y is replaced by y_o in equation (2), the value of y_o/b may be determined as

$$\frac{y_o}{b}=\frac{1}{(K^2R^2-R^2-1)^{1/2}} \tag{3}$$

Equation (2) may be rewritten as

$$C_p=1-\frac{K^2R^2\left(\frac{y}{y_o}\right)^2\left(\frac{y_o}{b}\right)^2}{1+\left(\frac{y}{y_o}\right)^2\left(\frac{y_o}{b}\right)^2(R^2+1)} \tag{4}$$

The drag on the nosepiece may then be determined as

$$C_{D,o}=\frac{2\pi}{\pi y_o^2}\int_0^{y_o}\left[1-\frac{K^2R^2\left(\frac{y}{y_o}\right)^2\left(\frac{y_o}{b}\right)^2}{1+\left(\frac{y}{y_o}\right)^2\left(\frac{y_o}{b}\right)^2(R^2+1)}\right]y\,dy \tag{5}$$

If $y'=y/y_o$, and thus $dy'=\frac{dy}{y_o}$, equation (5) may be written as follows:

$$C_{D,o}=2\int_0^1\left[1-\frac{K^2R^2(y')^2\left(\frac{y_o}{b}\right)^2}{1+(y')^2\left(\frac{y_o}{b}\right)^2(R^2+1)}\right]y'\,dy' \tag{6}$$

After integration, equation (6) becomes

$$C_{D,o}=1+\frac{K^2R^2}{(R^2+1)^2\left(\frac{y_o}{b}\right)^2}\log_e\left[1+(R^2+1)\left(\frac{y_o}{b}\right)^2\right]-\frac{K^2R^2}{R^2+1} \tag{7}$$

Equation (7) gives the drag coefficient of the positive-pressure portion of an ellipse in terms of the axis ratio of the ellipse. The fineness ratio f, which is defined as the ratio of the length to the base diameter of the positive-pressure nosepiece, may be written as

$$f=\frac{l}{d}=\frac{x_o}{2y_o} \tag{8}$$

or in terms of y_o/b from equation (3), equation (8) may be written as

$$f=\frac{R\left[1-\sqrt{1-\left(\frac{y_o}{b}\right)^2}\right]^{1/2}}{2\left(\frac{y_o}{b}\right)} \tag{9}$$

Equations (7) and (9) are a set of parametric equations in R for the drag coefficient of the positive-pressure nose region of a family of ellipses, and these nosepieces are equivalent to parabolic bodies of revolution. Results of computations

made by using equations (7) and (9) are presented in figure 3 as a plot of $C_{D,o}$ against the reciprocal of the fineness ratio of the paraboloids, $1/f$ or d/l. The computations reveal that for values of f greater than 1 the axis ratio of the parent ellipse is about 8 or greater. The most practical paraboloids will have fineness ratios of 5 or greater where R is 50 or greater. Since R is so large for these finer bodies an explicit relationship between C_D and f may be obtained by utilizing this fact that $R>>1$. If this approximation is made, the following equations for thin bodies result:

$$C_p \approx \frac{1-(y')^2}{\frac{(y')^2}{K^2-1}+1} \tag{10}$$

$$\left(\frac{y_o}{b}\right)^2 \approx \frac{1}{R^2(K^2-1)} \tag{11}$$

$$f \approx \frac{R\frac{y_o}{b}}{4} \tag{12}$$

Combining equations (11) and (12) results in

$$K^2-1=\frac{1}{16f^2} \tag{13}$$

Substituting equation (13) into equation (10) gives

$$C_p=\frac{1-(y')^2}{16f^2(y')^2+1} \tag{14}$$

Integrating equation (14) over the surface area gives the drag coefficient as

$$C_{D,o}=2\int_0^1 \frac{1-(y')^2}{16f^2(y')^2+1}y'dy'$$

$$=\frac{1}{16f^2}\left[\left(1+\frac{1}{16f^2}\right)\log_e(1+16f^2)-1\right] \tag{15}$$

As f goes to infinity, equation (15) becomes the exact solution for a paraboloid of infinite fineness ratio operating at zero cavitation number. This is true because as f goes to infinity the nosepiece becomes exactly parabolic and the pressure coefficient downstream becomes exactly uniformly

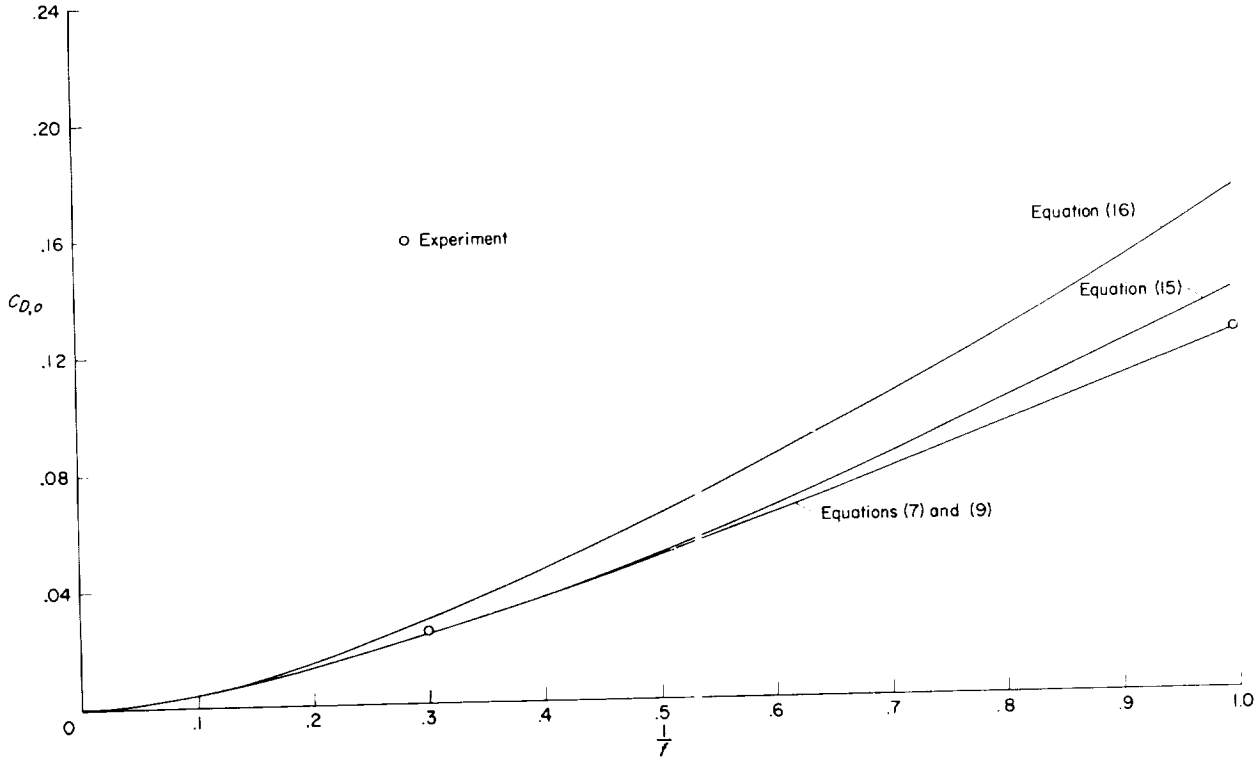

FIGURE 3.—Comparison of equations (7) and (9), (15), and (16) with experimental data.

zero. As f tends to infinity the drag coefficient given in equation (15) may be approximated by the following simpler equation:

$$C_{D,o} \approx \frac{1}{16f^2}\log_e 16f^2 \qquad (f \to \infty) \qquad (16)$$

Equation (16) is also the result which is obtained if the theoretical pressure distribution on a parabolic half-body is integrated over various lengths of the body. Equations (15) and (16) are plotted in figure 3 for comparison with equations (7) and (9). It may be seen that equation (15) is a very good approximation to the result given by equations (7) and (9) for values of $1/f$ less than 0.5. On the other hand, equation (16) is considerably higher than the other two results except at very small values of $1/f$.

Two-dimensional parabolic struts.—It is interesting to note that when the previous analytical method is applied to thin two-dimensional ellipses, equation (14) is also the result obtained for the pressure distribution on parabolic struts operating at zero cavitation number. The similarity in pressure distributions on two- and three-dimensional elliptical bodies in terms of appropriate cavitation numbers is discussed in reference 4. Actually, the pressure distributions on two- and three-dimensional parabolic bodies are identical at zero cavitation number only for the case of infinite fineness ratio. The fact that equation (14) is the approximate result for both two- and three-dimensional parabolic bodies reveals that the analogy pointed out in reference 4 is closely approximated for more useful fineness ratios. The integration of equation (14) over the frontal area of a two-dimensional parabola gives the form-drag coefficient at zero cavitation number as

$$C_{D,o} = \frac{1}{16f^2}\left[\frac{16f^2+1}{4f}(\tan^{-1}4f) - 1\right] \qquad (17)$$

For thin struts (that is, as f becomes very much greater than unity), equation (17) reduces to the result given in reference 1:

$$C_{D,o} = \frac{\pi}{8f}$$

EXPERIMENT

MODELS

The models used in the experimental investigation are shown in figure 4. The models are paraboloids generated by revolving the line $y = \frac{d}{2}\sqrt{\frac{x}{l}}$ about the X-axis. The model shown on the left is 4.5 inches long and has a diameter-length ratio d/l of 1.0. The indented structure at the base of the model on the left was necessary to house the instrumentation, but this structure lies within the cavity during operation and has no influence on the forebody. The model on the right is 18.5 inches long with a base diameter of 5.5 inches, resulting in a diameter-length ratio d/l of 0.3.

APPARATUS AND PROCEDURE

Facility.—The models were investigated in the Langley high-speed hydrodynamics facility. The tank and high-speed carriage are described in detail in references 7 and 8. The carriage is capable of speeds up to 250 fps.

Model support and instrumentation.—The models were supported on a sting with a strain-gage balance housed inside the model as shown in figure 5. The models were made watertight by connecting the base of the model to the sting with a watertight bellows. The balance, which measured only drag for these zero-yaw tests, was located within the models rather than above water in order to eliminate the supporting-strut drag tares. Also located within the models were strain-gage pressure cells connected to pressure orifices along the surface of the model and one on the base so as to be within the cavity. The locations of the surface pressure orifices are given in figure 5. The electrical output leads from the pressure cells and balance were passed out of the model through a hole along the longitudinal axis of the sting.

The sting was supported by means of the tri-strut arrangement shown in figures 6 and 7. The tri-strut structure was connected to the support cylinder of the towing-carriage boom, as may be seen in figure 7.

Ventilation system.—The ventilation probe and ventilation tube shown in figure 6 were used to achieve ventilation of the base cavity formed behind the model. The upper end of the ventilation tube was connected to a 75-psi compressed-air tank on the carriage. With the air supply on, almost complete ventilation was achieved. This forced air apparently enlarged both the cavity formed at the base of the model and the cavity formed aft of the ventilation tube, with the result

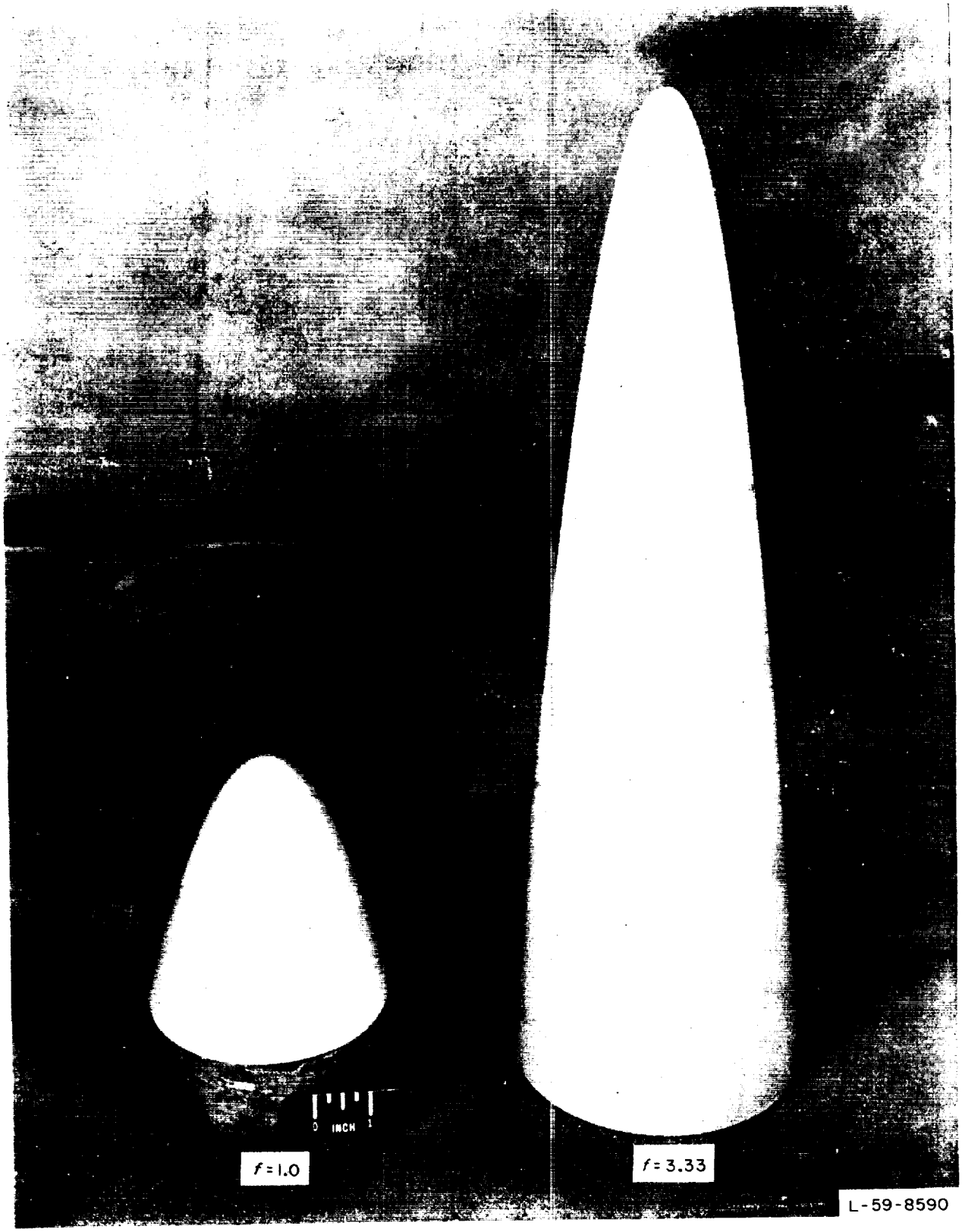

FIGURE 4. The models.

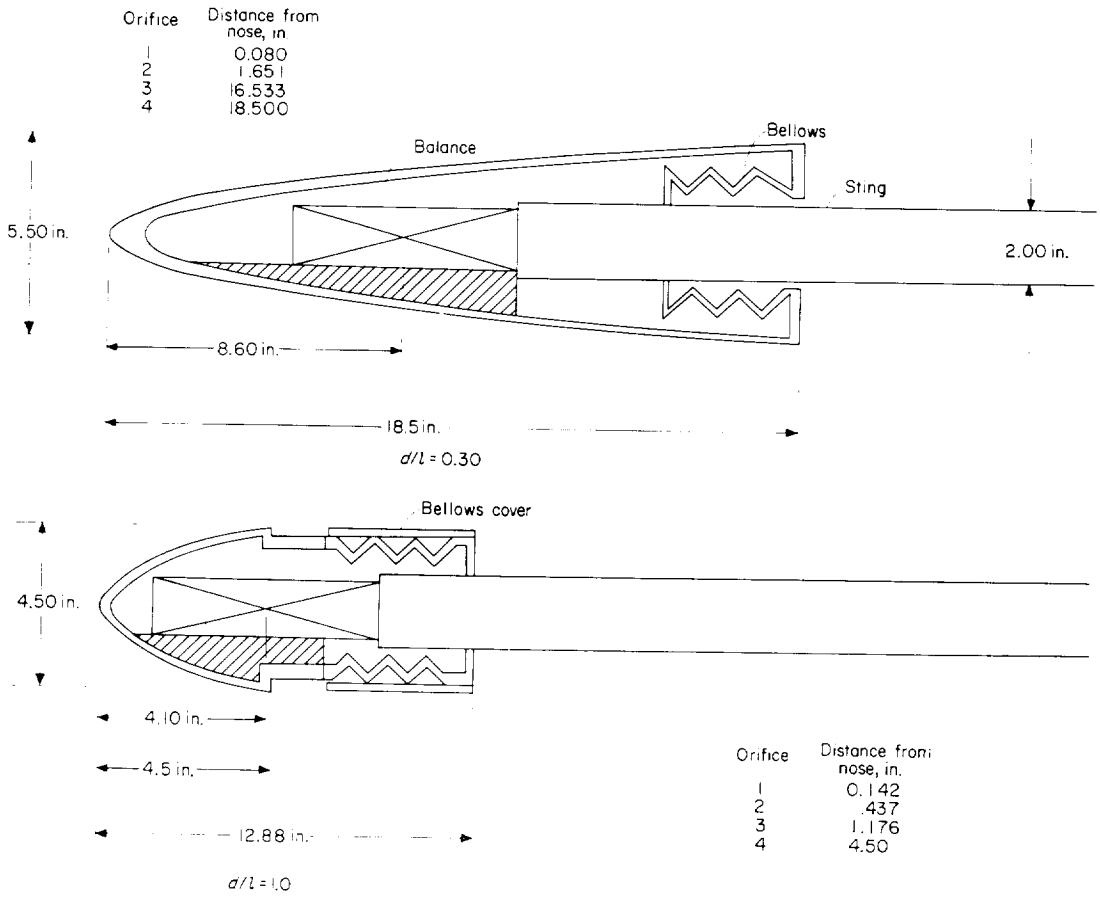

FIGURE 5.—Details of model connection to sting. Pressure orifice locations are given in distance along longitudinal axis of the model.

that the two cavities connected and the tube cavity extended rearward to the probe. The probe then opened the entire cavity system to the atmosphere. Without the forced air only partial ventilation was achieved.

Photographs and recording equipment.—Photographs were taken of the model and cavity at selected stations along the tank. Carriage speed was determined at each of these photographic stations by electronically measuring the time for the model to pass a distance of 10 feet. The balance and pressure-cell outputs were recorded on oscillographs inside the carriage. A magnetic device was employed to indicate on the balance record when the carriage passed a photographic station and thus to provide synchronization between the measurements of speed, force, and pressure and the photographs.

Test conditions.—The models were investigated at a constant depth of 14 inches. At this depth it was estimated that free-surface and boundary effects on the measured drag of the models would be negligible. The speed range utilized in the investigation was from 130 to 190 fps. The density of the tank water used in computing the force coefficients was 1.94 lb-sec^2/ft^4. The kinematic viscosity during the investigation was 1.42×10^{-5} ft^2/sec.

ACCURACY

The accuracy of the quantities measured is estimated to be within the following limits:

Drag, lb	±5
Speed, fps	±0.15
Pressure, lb/sq ft	±20

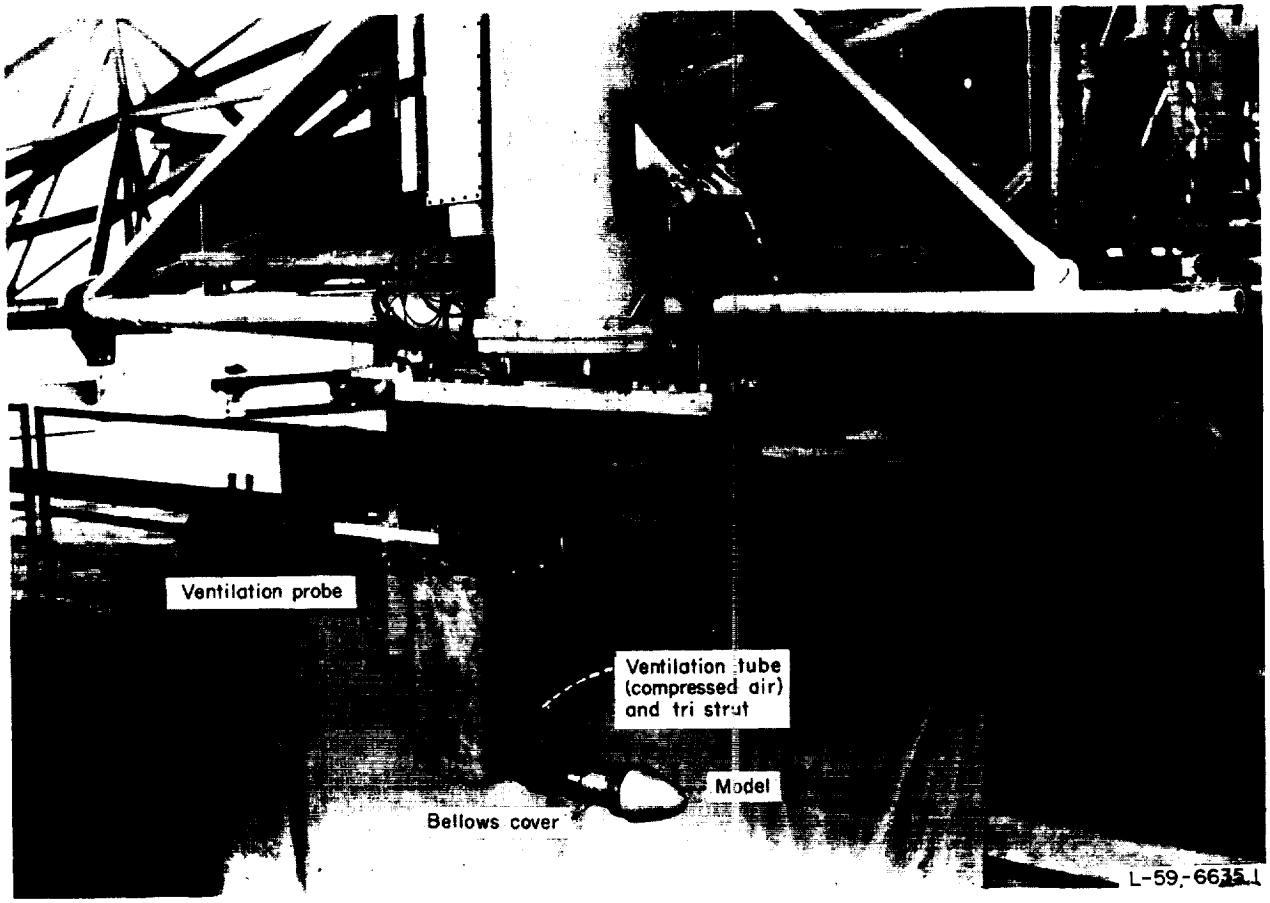

FIGURE 6.—Model support and ventilation system.

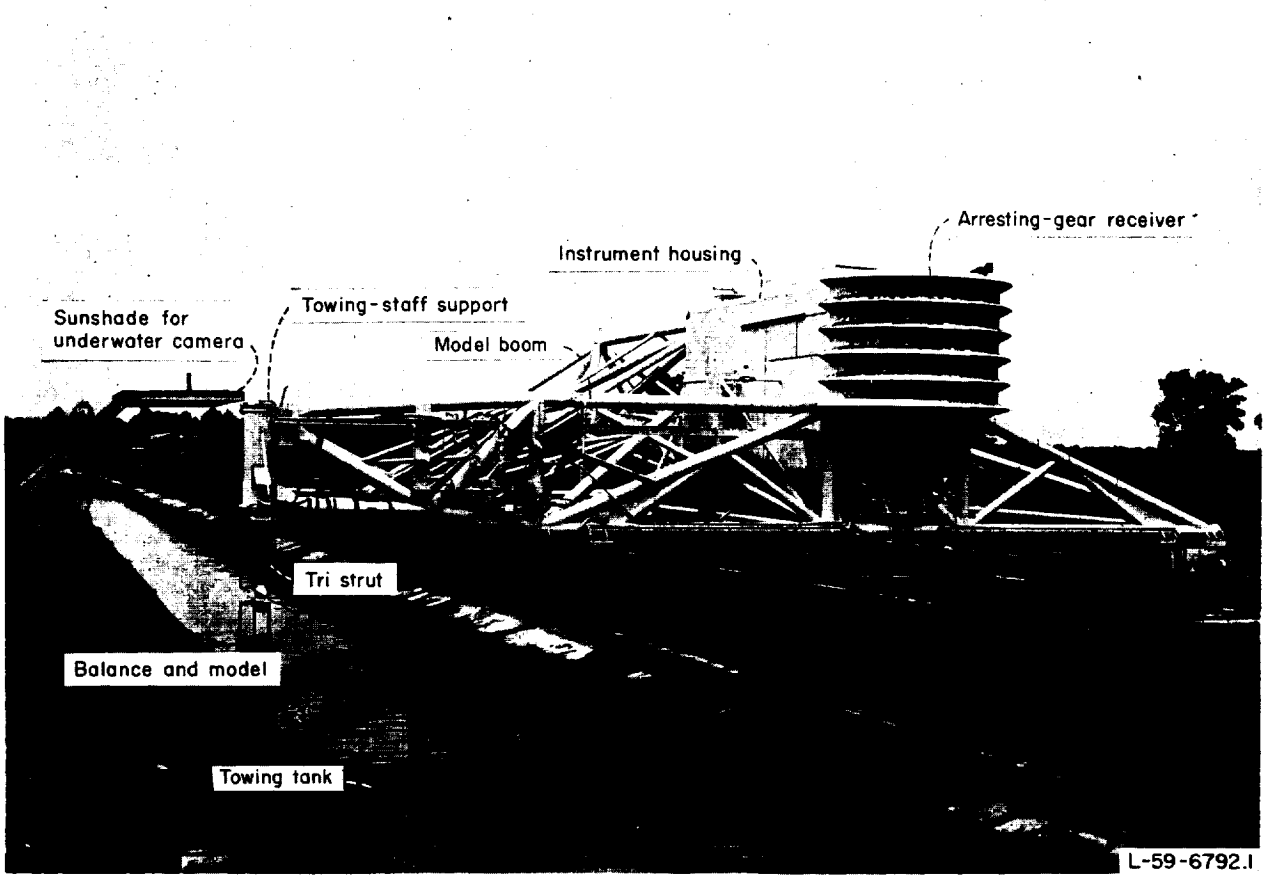

FIGURE 7.—The high-speed carriage with model attached.

RESULTS AND DISCUSSION

FLOW CHARACTERISTICS

Figures 8(a) and 8(b) are typical photographs taken of the models when they were operating with ventilated base cavities. The cavitation number for this ventilated type of operation was about 0.01 for all observations of both models.

Although the tri-strut support extended into the upper portion of the long cavities formed at the base of the models; it is believed that this strut interference had negligible influence on the observed drag of the bodies.

DRAG

The skin-friction drag was calculated and removed from the total measured drag in order to obtain the net form drag. In reference 9 it is shown that the skin friction on bodies of revolution with fairly uniform pressure distribution may be adequately calculated by using flat-plate boundary-layer theory. Thus, the skin friction

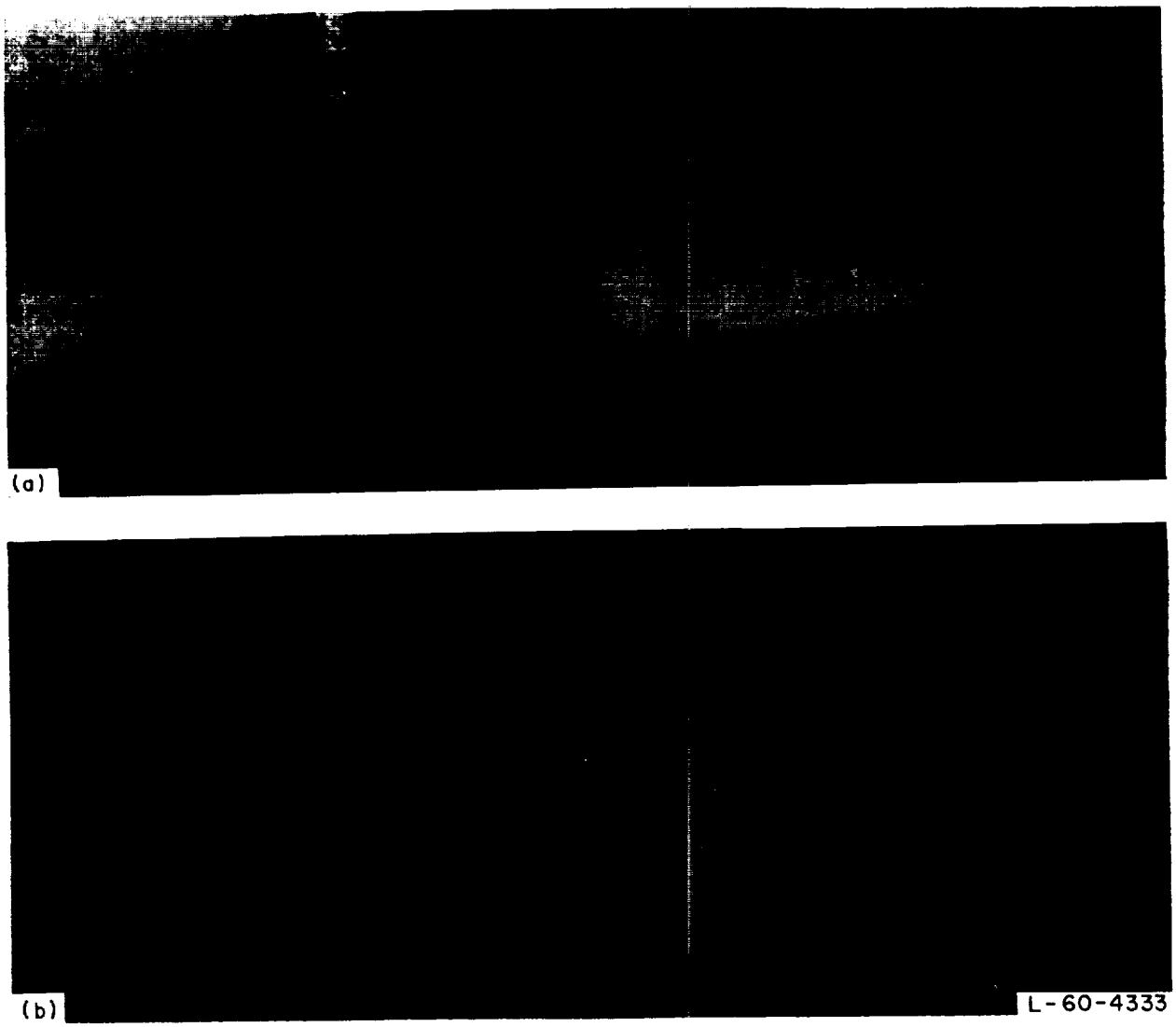

(a) $f = 3.33$; $V = 148$ fps.
(b) $f = 1.0$; $V = 174$ fps.

FIGURE 8. Photographs of models with ventilated base cavities. $\sigma = 0.01$.

was calculated by assuming turbulent flow over the entire wetted surface and using the turbulent skin-friction coefficient given for a flat plate in reference 10. The resulting values are approximately the same as those calculated for mixed flow on the assumption that transition occurs at a Reynolds number of 3×10^5. The calculated skin friction for the range of variables in the present investigation amounted to about 4 percent of the total measured drag for the model with $f=1$ and about 40 percent for the model with $f=3.33$.

The form drag obtained is plotted against speed for each model in figure 9. The cavitation number σ, based on the measured cavity pressure, is also indicated for each point. It may be noted that the measured cavitation numbers are indeed very nearly zero but not exactly zero.

From the data presented in figure 9, the form-drag coefficient $C_D=\frac{1}{2}\rho V^2S$ was computed for each point. Since these data were not measured at exactly zero cavitation number, the measured value of C_D must be corrected for the base cavitation number in order to obtain the form drag coefficient at zero cavitation number. This correction was made by assuming that $C_{D,o}=C_D-\sigma$, as discussed in the section on theory. The values of $C_{D,o}$ obtained in this manner are plotted against speed in figure 10. It can be seen that the value of $C_{D,o}$ is independent of speed.

It is recognized that the model with $f=1$ is not sufficiently thin for the equation $C_D=C_{D,o}+\sigma$ to be a good approximation. For small cavitation numbers, reference 4 gives the drag coefficient of a cone with $C_{D,o}$ about equal to 0.13 as $C_D=C_{D,o}+0.87\sigma$. On the assumption that cones and paraboloids are comparable on the basis of $C_{D,o}$ alone, a better value of $C_{D,o}$ for the paraboloid with $f=1$ may be $C_{D,o}=C_D-0.87\sigma$. If such a relationship is more nearly correct than $C_{D,o}=C_D-\sigma$, the data shown in figure 10 for the model with $f=1$ are about 1 percent too low.

The $C_{D,o}$ values of 0.025 for $f=3.33$ and 0.125 for $f=1.0$ are compared with theory in figure 3. It may be seen that the agreement between the experimental values and the results given by equations (7) and (9) is excellent.

In figure 11 the results given by equations (7)

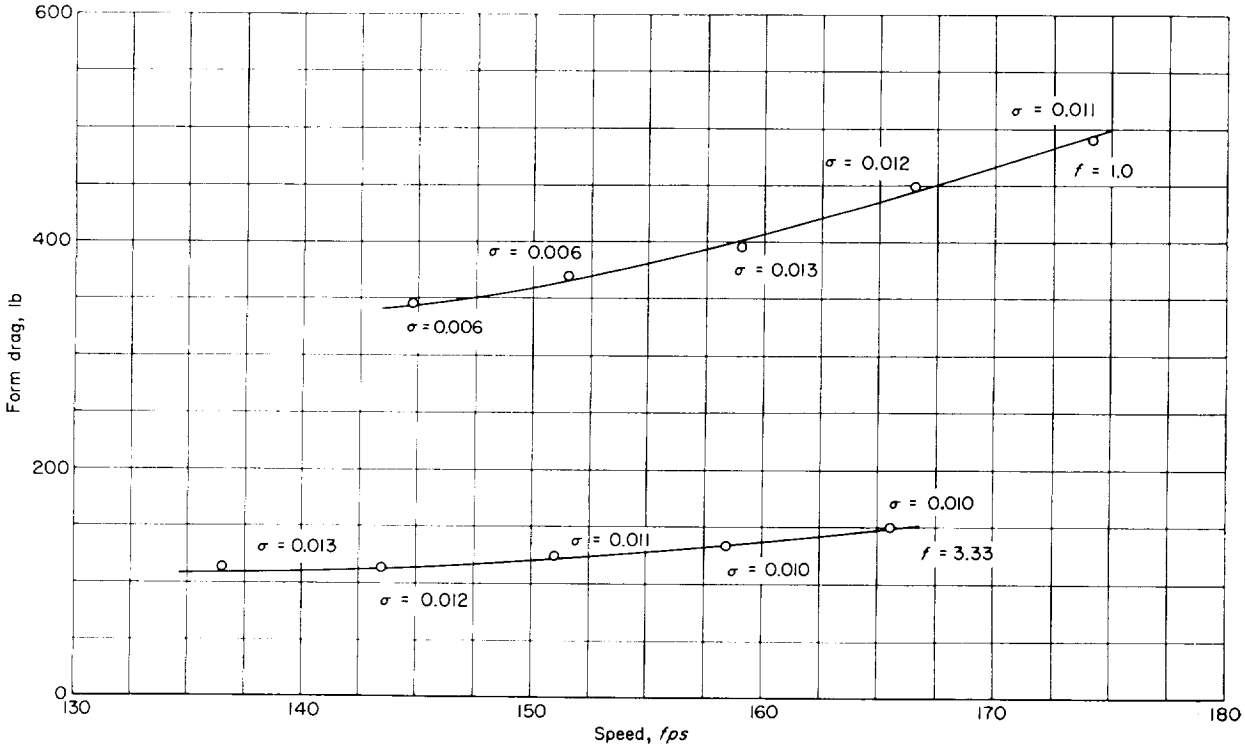

FIGURE 9.—Model form drag.

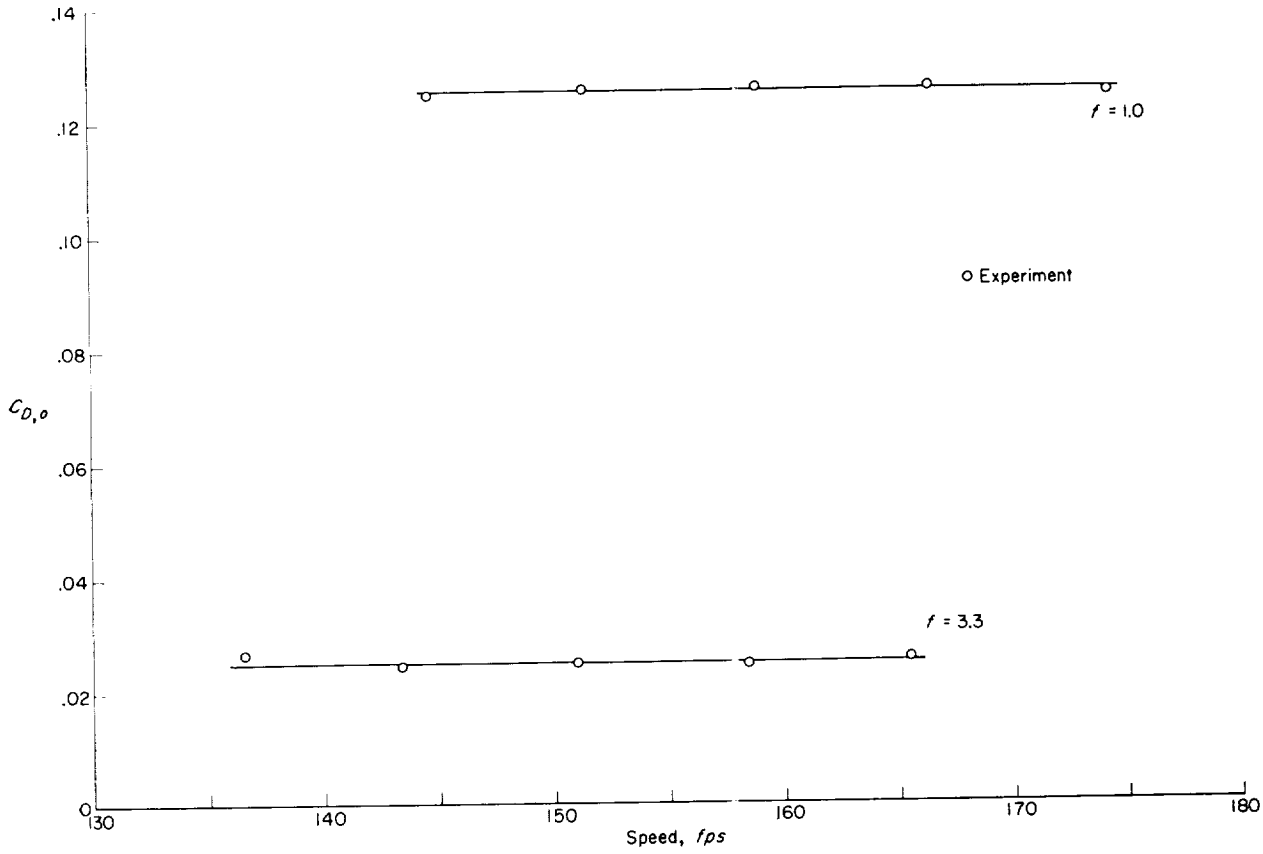

FIGURE 10. -Variation of drag coefficient at zero cavitation number with speed for parabolic bodies.

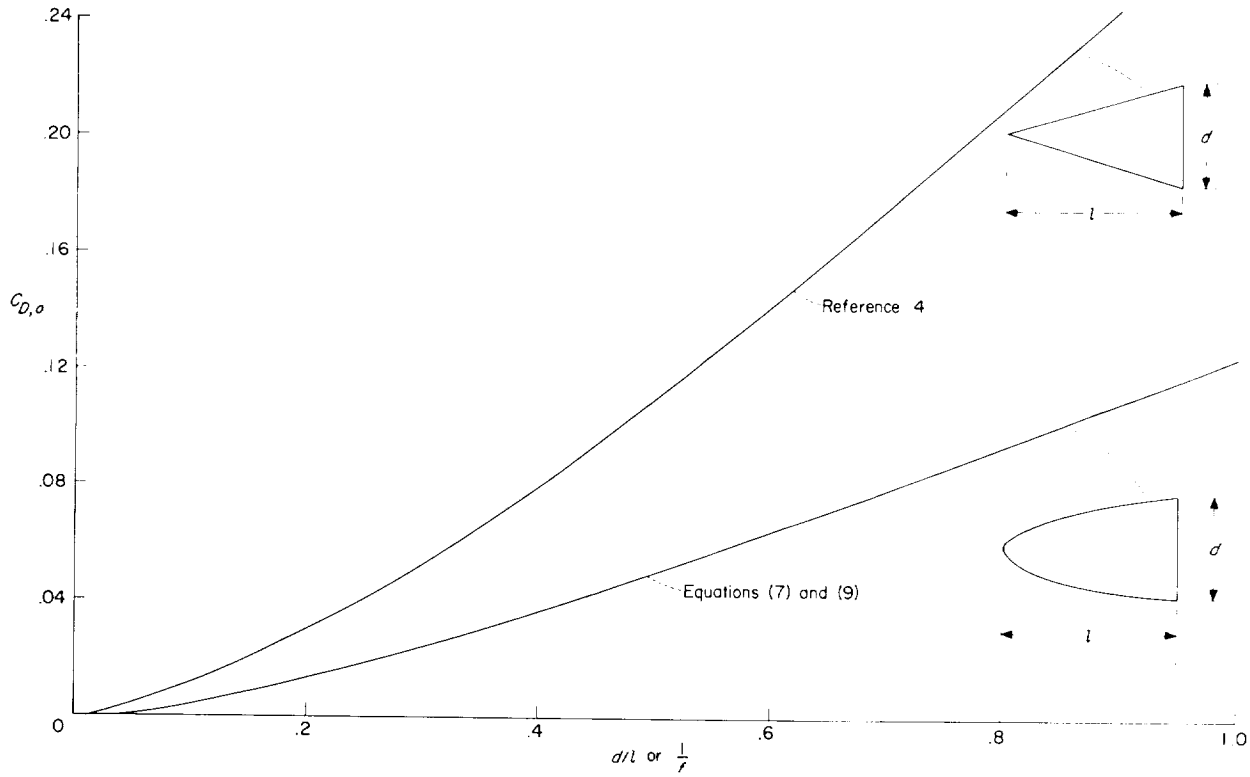

FIGURE 11.—Comparison of theoretical form-drag coefficients of cones and parabolas at zero cavitation number.

and (9) (and the experimental data) are compared with the theoretical results for cones obtained from reference 4. Figure 11 shows that the theoretical form-drag coefficient at zero cavitation number for a given diameter-length ratio is about twice as high for a cone as for a paraboloid.

The total drag on paraboloids of revolution operating at zero cavitation number may be obtained by using the results presented in figure 3 and adding the skin friction as calculated from flat-plate theory.

PRESSURES

The measured surface pressures obtained during the investigation are plotted and compared in figure 12 with the theoretical pressure distribution given by equation (14). The agreement between experiment and theory is very good for both models.

CONCLUSIONS

Force tests were made on two parabolic bodies having fineness ratios of 1.0 and 3.33 and the results were compared with theoretical results. The investigation may be summarized with the following conclusions:

1. The approximate theoretical expressions derived for the pressure distribution and form drag on paraboloids operating at zero cavitation number and zero angle of yaw are in excellent agreement with the experimental data obtained.

2. The theoretical form-drag coefficient of paraboloids operating at zero cavitation number is about one-half the form-drag coefficient of cones having the same fineness ratio.

LANGLEY RESEARCH CENTER,
NATIONAL AERONAUTICS AND SPACE ADMINISTRATION,
LANGLEY FIELD, VA., *July 28, 1960.*

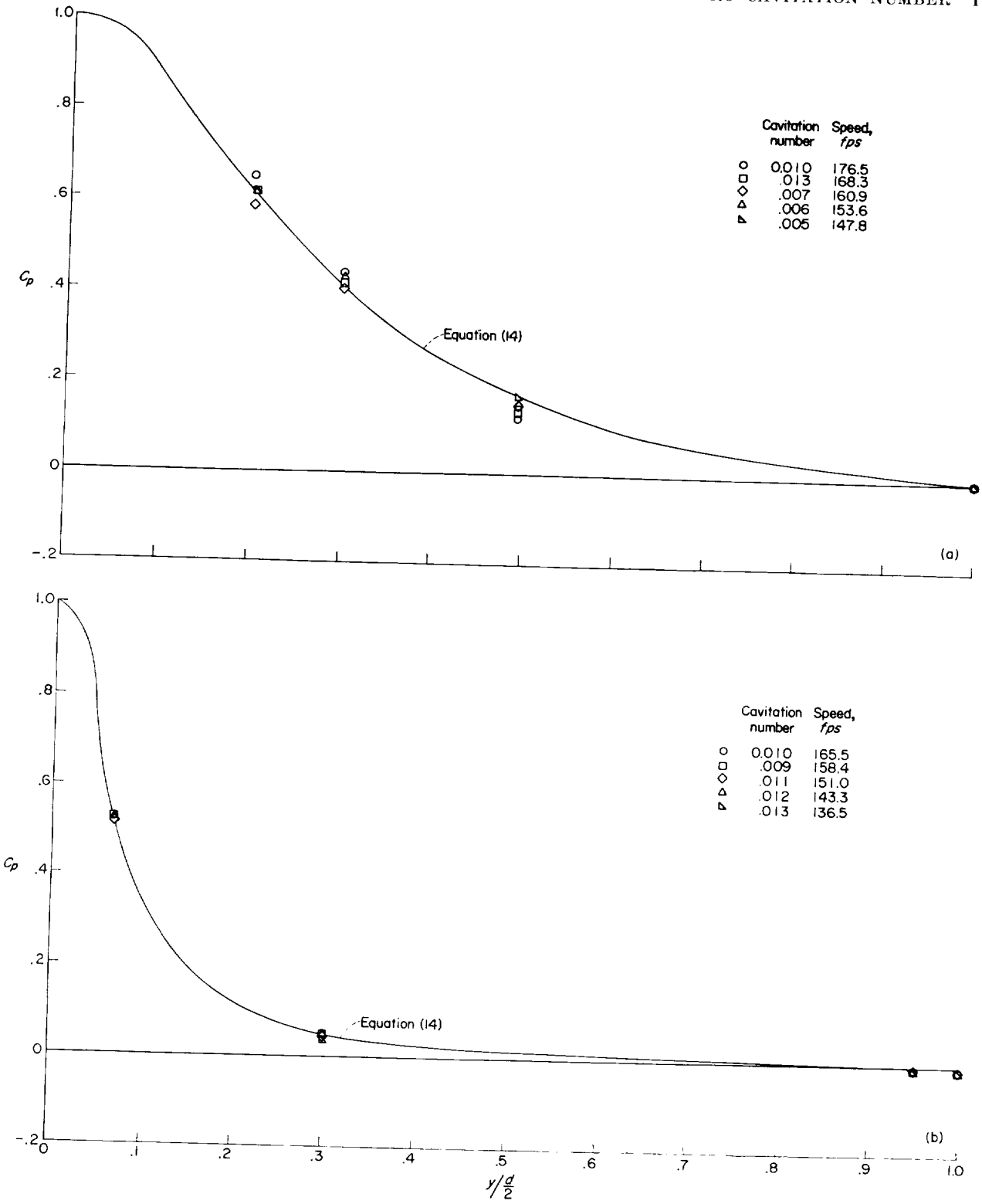

(a) $f = 1.0$.
(b) $f = 3.33$.

FIGURE 12. - Comparison of theoretical and experimental pressure distributions.

REFERENCES

1. Tulin, M. P.: Supercavitating Flow Past Foils and Struts. Cavitation in Hydrodynamics, NPL (Teddington, England), 1956, 16 p. 1–16 p. 19.
2. Levinson, N.: On the Asymptotic Shape of the Cavity Behind an Axially Symmetric Nose. Ann. Math, vol. 47, 1946, p. 704.
3. Münzner, H., and Reichardt, H. (A. H. Armstrong, trans.): Rotationally Symmetrical Source-Sink Bodies With Predominantly Constant Pressure Distribution. Translation No. 1/50, Armament Res. Establishment (British), Apr. 1950.
4. Armstrong, A. H. (appendix by C. G. Clarke): Drag Coefficients of Wedges and Cones in Cavity Flow. Rep. 21/54, Armament Res. Establishment (British), Aug. 1954.
5. Milne-Thomson, L. M.: Theoretical Hydrodynamics. Second ed., Macmillan and Co., Ltd., 1949.
6. Rouse, Hunter, and McNown, John S.: Cavitation and Pressure Distribution—Head Forms at Zero Angle of Yaw. Studies in Eng. Bull. 32, State Univ. of Iowa, 1948.
7. Christopher, Kenneth W.: Investigation of the Planing Lift of a Flat Plate at Speeds up to 170 Feet Per Second. NACA TN 3951, 1957.
8. Johnson, Virgil E., Jr., and Rasnick, Thomas A.: Investigation of a High-Speed Hydrofoil With Parabolic Thickness Distribution. NASA TN D–119, 1959.
9. Mottard, Elmo J., and Loposer, J. Dan: Average Skin-Friction Drag Coefficients From Tank Tests of a Parabolic Body of Revolution (NACA RM–10). NACA Rep. 1161, 1954. (Supersedes NACA TN 2854.)
10. Schoenherr, Karl E.: Resistance of Flat Surfaces Moving Through a Fluid. Trans. Soc. Naval Arch. and Marine Eng., vol. 40, 1932, pp. 279–313.

U.S. GOVERNMENT PRINTING OFFICE: 1961